Lectures on Mathematical Aspects of Physiology
Charles S. Peskin

II. The Inner Ear

5. Fluid dynamics of the cochlea: Formulation of a model and analysis of the inviscid case. In this section, we shall describe a mathematical model of the inner ear (cochlea), and we shall analyze the special case in which there is no fluid viscosity. The viscous case will be studied in the next section.

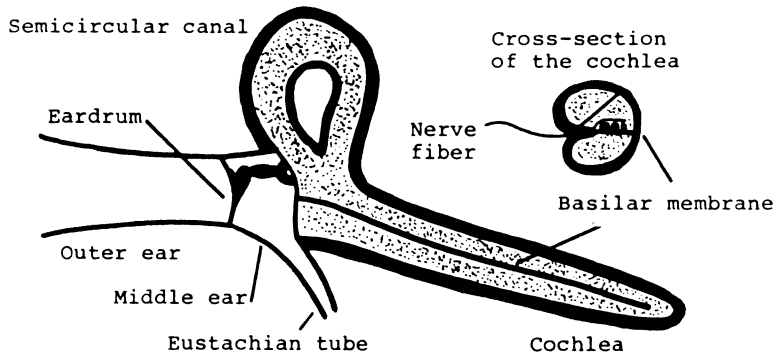

FIGURE 5.1. The cochlea (redrawn after von Bekesy). Only one of the three semicircular canals is shown and the cochlea has been drawn straightened out.

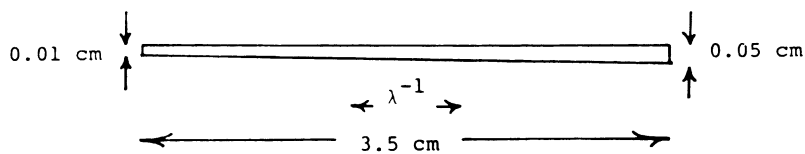

FIGURE 5.2. Dimensions of the basilar membrane.

The anatomy of the cochlea and its relationship to the other parts of the ear are shown in Figure 5.1. Unlike the outer and middle ears, the cochlea is filled with (essentially) water. It is divided into two main parts by an elastic structure called the basilar membrane which is shown in Figure 5.2.

The waves that propagate in the cochlea are not sound waves in the ordinary sense. Although the kinetic energy is stored in the fluid, the

Lectures in Applied Mathematics 19, 1981

elastic energy is stored in the basilar membrane, and compression of the fluid can be entirely neglected. In other words, we are dealing with surface waves, like ripples on the surface of a pond. This analogy can be made very precise, as we shall see.

Practically everything that we know about the waves that propagate in the cochlea was discovered by Georg von Bekesy, who observed these waves directly with a microscope using stroboscopic illumination. von Bekesy also constructed physical models of the cochlea, and he used these models to determine which properties of the cochlea are essential to its function. We shall give a brief summary of von Bekesy's discoveries:

1. The response of the cochlea to a steady pure tone is a traveling wave.

2. The amplitude of this wave is a steady function of position that rises gradually to a unique maximum from which it decays more rapidly.

3. When the frequency of the stimulus is changed, the amplitude function does not change shape, but it translates to a new position. The position of the maximum varies as the negative logarithm of the stimulus frequency. Since the fibers of the auditory nerve are distributed along the length of the basilar membrane, this means that sounds of different frequencies stimulate different groups of nerve fibers.

4. The compliance per unit length of the basilar membrane varies with position as $e^{\lambda x}$, where $\lambda^{-1} = 0.7$ cm. (The definition of compliance is volume displaced per unit pressure difference.)

5. Under a point load the basilar "membrane" actually deforms as a plate, not as a membrane. Moreover, there is no resting tension in the basilar membrane.

6. The fluid in the cochlea is necessary for the traveling wave. If the fluid is removed, all parts of the basilar membrane vibrate synchronously in response to an imposed pressure oscillation. This strongly suggests that the mass of the basilar membrane is not important and that the important mass in the cochlea is that of the fluid.

7. Although fluid is needed, the depth of the fluid is certainly not critical. Traveling waves can be seen in a drop of fluid placed on the basilar membrane. In physical models, the depth of fluid can be adjusted. Increasing the depth beyond its normal value has no effect on the traveling wave.

8. The curvature of the cochlea is also not critical, since the traveling wave can be reproduced in straight physical models.

9. The traveling wave takes on a form, and even a direction of propagation, that are not very sensitive to the mode of stimulation of the cochlea. The most spectacular example of this is the paradoxical

wave, traveling towards the source, that can be elicited by putting a sinusoidal source at the far end of the cochlea.

In any fluid dynamical problem, it is important to know the orders of magnitude of various physical parameters. For the human cochlea, we have the following lengths.

Length of basilar membrane: 3.5 cm

Length-constant (λ^{-1}) of the basilar membrane: 0.7 cm

Width of the basilar membrane: 0.01–0.05 cm

Depth of each half-cochlea: 0.2–0.1 cm

The fluid has

Density (ρ): 1 gm/cm^3

Viscosity (μ): 0.02 (cm^2/sec)(gm/cm^3)

and the stimulating sound is characterized by

Frequency (f): 20,000–20 cycles/sec.

From the density, viscosity, and frequency, we can calculate a boundary layer thickness which gives a rough estimate of how far viscous effects extend into the fluid from the boundaries:

Boundary layer thickness $(\mu/\rho f)^{1/2}$: 0.001–0.03 cm.

If we had used the angular frequency $\omega = 2\pi f$, then the boundary layers would look thinner by a factor $\sqrt{2\pi}$.

For reasons that will become clear as we proceed, the natural unit of length for the cochlea is $\lambda^{-1} = 0.7$ cm, which is the distance that it takes for the compliance (per unit length) of the basilar membrane to change by a factor of e. In comparison with this, the basilar membrane is long and narrow, the depth of the cochlea is moderate, and the boundary layers are thin. In fact the boundary layers are also thin compared to the depth. In the worst case this ratio is 1:3 but in the middle range of frequencies it is more like 1:30.

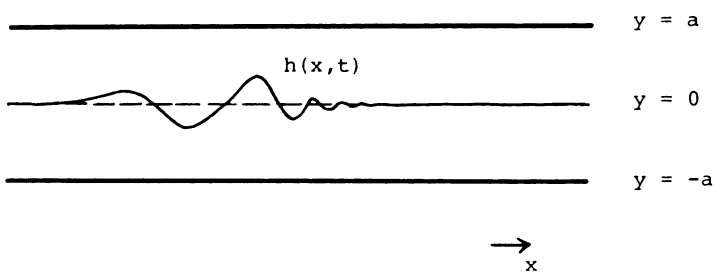

FIGURE 5.3. Two-dimensional model of the cochlea.

We shall now describe the two-dimensional model that will be used in this section and the next; see Figure 5.3. The model occupies the strip $-a \leq y \leq a$ in the (x, y) plane; it is infinite in both the positive and negative x-directions. The undisturbed position of the basilar membrane

is given by $y = 0$, and its displacements are given by $y = h(x, t)$. The walls at $y = \pm a$ are rigid, and the source of vibration is applied at $x = -\infty$. The velocity and pressure of the fluid are denoted (u, v) and p.

We shall state the equations of the model first, and then we shall describe the various assumptions and approximations that are implicit in these equations.

In the fluid domain, $0 < |y| < a$, we have

$$\rho \partial u/\partial t + \partial p/\partial x = \mu \Delta u, \tag{1}$$

$$\rho \partial v/\partial t + \partial p/\partial y = \mu \Delta v, \tag{2}$$

$$\partial u/\partial x + \partial v/\partial y = 0. \tag{3}$$

At the rigid boundaries, $y = \pm a$,

$$u = 0, \tag{4}$$

$$v = 0 \tag{5}$$

and, at the basilar membrane, $y = 0$, we have the boundary conditions

$$u = 0, \tag{6}$$

$$v = \partial h/\partial t, \tag{7}$$

$$[p] = -s_0 e^{-\lambda x}(h + \beta \partial h/\partial t). \tag{8}$$

In these equations, Δ stands for the Laplace operator

$$\Delta = \partial^2/\partial x^2 + \partial^2/\partial y^2 \tag{9}$$

and [ ] stands for the jump in a quantity across $y = 0$, so that

$$[p] = p(x, 0^+, t) - p(x, 0^-, t) = \lim_{\varepsilon \downarrow 0} (p(x, \varepsilon, t) - p(x, -\varepsilon, t)). \tag{10}$$

Thus $[p]$ is the load on the basilar membrane.

Equations (1)–(3) are the linearized equations of a viscous incompressible fluid with viscosity μ and density ρ. The linearization is that the convection terms $\mathbf{u} \cdot \nabla \mathbf{u}$, which arise from the displacement of fluid particles, have been omitted. In the same spirit, we have applied the boundary conditions of the basilar membrane to its undisturbed location, $y = 0$. Thus we have assumed that the displacements of the fluid particles (and hence of the basilar membrane) are small compared to the distances over which the velocity of the fluid changes appreciably.

At the threshold of hearing it has been estimated that the displacements of the eardrum are as small as the diameter of the nucleus of a hydrogen atom. (Of course, such a small displacement of a single molecule would be lost in thermal noise, but the correlated displacements of $\sim 10^{23}$ molecules might be detectable.) Even if this estimate of the displacement of the eardrum is not very accurate, and even allowing

for amplification in the cochlea and for larger displacement with louder sounds, there is still a long way to go before displacements of fluid particles in the cochlea can be regarded as appreciable.

There are nonlinearities in hearing, however, and it is an open question whether these should be attributed to the fluid mechanics or to the nervous system. In these sections we assume that the fluid mechanics are linear.

In writing the boundary conditions we have assumed that the outer walls are fixed and that the basilar membrane moves in the vertical direction only. The conditions on v, (5) and (7), just assert that the fluid cannot penetrate the boundaries. These conditions hold whether or not the fluid is viscous. The conditions on u, (4) and (6), are the no-slip conditions that hold in the viscous case only.

Finally we come to equation (8), which models the basilar membrane itself. The left-hand side gives the load on the basilar membrane [p]. It might appear that we should add to this the vertical component of the viscous stress $\mu[\partial v/\partial y]$. Using the boundary condition (6) and the continuity equation (3), we see that $\partial v/\partial y = 0$ on each side of the basilar membrane, so the missing term is actually zero.

The right-hand side of (8) gives the response to the load on the basilar membrane in terms of the membrane displacement $h(x, t)$. The expression that appears there is based on the following assumptions:

(i) The membrane has zero mass.

(ii) There is no elastic coupling between points at different values of x along the basilar membrane.

(iii) Each part of the membrane responds to its load like a viscoelastic system with a stiffness proportional to $e^{-\lambda x}$ and a time-constant β that is independent of x.

The assumption that the membrane has zero mass is based on the observation that the traveling wave disappears and the membrane vibrates synchronously when the fluid is removed. The lack of longitudinal elastic coupling in the model can be justified by considering a narrow plate that is clamped along its edges. The exponential dependence of stiffness on position comes directly from von Bekesy's measurements of compliance.

The existence of the friction term, $\beta \partial h/\partial t$, is pure conjecture, however. In the analysis that follows, we shall see why it is essential to have some dissipative mechanism in the model, but that role could be played by fluid viscosity instead of membrane friction.

During the rest of this section, we shall study the case $\mu = 0$. We start by simplifying the problem as follows:

First, look for solutions in which $(u, v) = \text{grad } \phi e^{i\omega t}$, where ϕ satisfies the antisymmetry condition $\phi(x, y) + \phi(x, -y) = 0$. This gives us a

problem in which ϕ is the only unknown and the domain is the lower half-cochlea $-a \leqslant y \leqslant 0$:

$$-\omega^2\phi + \frac{s_0 e^{-\lambda x}}{2\rho}(1 + i\omega\beta)\frac{\partial\phi}{\partial y} = 0, \qquad y = 0, \tag{11}$$

$$\Delta\phi = 0, \qquad -a < y < 0, \tag{12}$$

$$\frac{\partial\phi}{\partial y} = 0, \qquad y = -a. \tag{13}$$

If the coefficient $(s_0 e^{-\lambda x}/2\rho)(1 + i\omega\beta)$ were replaced by the constant g, this would be precisely the problem of gravity waves of small amplitude in a channel of finite depth. In our case, the coefficient corresponding to g depends on x because the stiffness of the basilar membrane is not constant, and it is also complex because of the basilar membrane friction. We can get rid of the x-dependence by applying the conformal mapping

$$X = e^{\lambda x}\cos\lambda y, \tag{14}$$

$$Y = e^{\lambda x}\sin\lambda y. \tag{15}$$

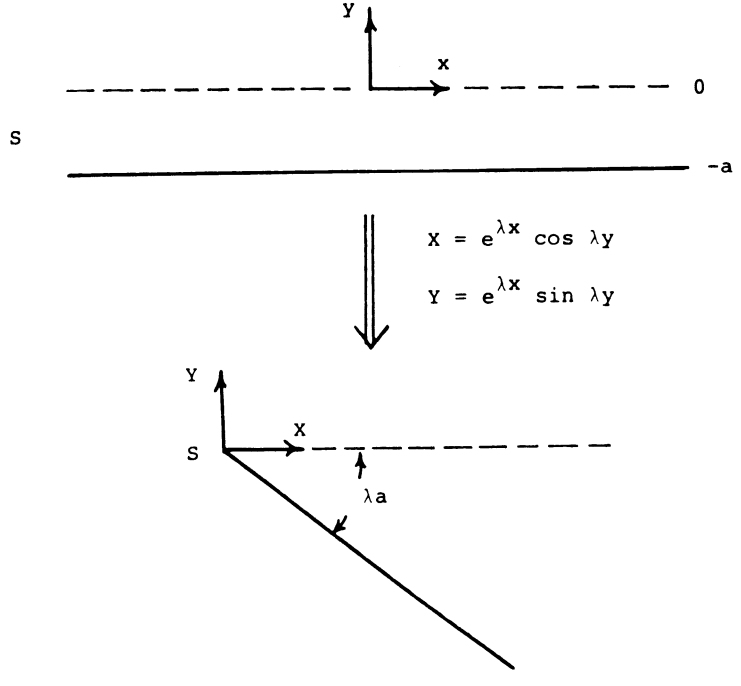

FIGURE 5.4. Conformal mapping of the lower half-cochlea onto a wedge. The source S at $x = -\infty$ is mapped at $X = Y = 0$.

This mapping takes the strip $-a < y < 0$ into the wedge $-\tan(\lambda a) < (Y/X) < 0$, as shown in Figure 5.4. Note that the source at $x = -\infty$ is mapped to $X = Y = 0$. The reason for considering this mapping becomes clear when we notice that, along $y = 0$,

$$\frac{\partial \phi}{\partial y} = \frac{\partial \Phi}{\partial X}\frac{\partial X}{\partial y} + \frac{\partial \Phi}{\partial Y}\frac{\partial Y}{\partial y} = 0 + \frac{\partial \Phi}{\partial Y}\lambda e^{\lambda x}. \tag{16}$$

This factor $e^{\lambda x}$ introduced by the mapping will just cancel the factor $e^{-\lambda x}$ that appears in the boundary condition (11).

Finally, consider the special case $\lambda a = \pi/2$. In this case the boundary condition (13) becomes simply $(\partial\Phi/\partial X) = 0$ along $X = 0$, and we can guarantee that this condition will be satisfied if we extend Φ as an even function about $X = 0$. The condition $\lambda a = \pi/2$ makes our model cochlea too deep by a factor of about 5, but we rely on von Bekesy's observation that the depth can be increased without changing the wave motion that occurs.

Accordingly, we are led to the following problem on $Y < 0$:

$$-\omega^2\Phi + \frac{s_0\lambda}{2\rho}(1 + i\omega\beta)\frac{\partial \Phi}{\partial Y} = \Phi_0\omega_0^2\delta(X), \qquad Y = 0, \tag{17}$$

$$\Delta\Phi = 0, \qquad Y < 0, \tag{18}$$

$$\Phi \to 0, \qquad Y \to -\infty, \tag{19}$$

in which we have explicitly put in the source at the origin. The source strength $\Phi_0\omega_0^2$ has been written this way to make the units consistent in (17). (In checking the units, recall that X and Y are dimensionless, while Φ has the same units as ϕ.) It will be convenient to set

$$\omega_0^2 = s_0\lambda/2\rho. \tag{20}$$

Equations (17)–(19) are exactly the equations for ripples on the surface of a deep pond with surface friction. The ripples are generated by an oscillating line source on the surface. This is an old problem that was solved by Lamb, but some new phenomena will appear when we transform the solution back to the original variables.

One can verify by direct substitution that the integral

$$\Phi(X, Y) = \frac{\Phi_0\omega_0^2}{2\pi}\int_{-\infty}^{\infty} \frac{e^{i\xi X + |\xi| Y}}{-\omega^2 + \omega_0^2(1 + i\omega\beta)|\xi|}\, d\xi \tag{21}$$

satisfies equations (17)–(19). To check this, first note that the integrand satisfies (18) and (19) for each ξ. Then substitute the integral in (17) and recall that

$$\delta(X) = \frac{1}{2\pi}\int_{-\infty}^{\infty} e^{i\xi X}\, d\xi. \tag{22}$$

We shall pull an interesting term out of (21) and then show that the rest of the integral is small. To do this, we begin by writing $\Phi = \Phi_1 + \Phi_2$, where

$$\Phi_1 = \frac{1}{1 + i\omega\beta} \frac{\Phi_0}{2\pi} \int_0^\infty \frac{e^{i\xi X + \xi Y}}{\xi - \zeta_0} \, d\xi, \tag{23}$$

$$\Phi_2 = \frac{1}{1 + i\omega\beta} \frac{\Phi_0}{2\pi} \int_0^\infty \frac{e^{-i\xi X + \xi Y}}{\xi - \zeta_0} \, d\xi \tag{24}$$

and where

$$\zeta_0 = \omega^2/\omega_0^2(1 + i\omega\beta). \tag{25}$$

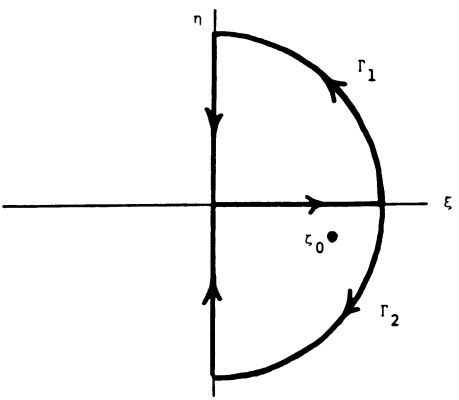

FIGURE 5.5. Contours used to rewrite Φ_1 and Φ_2. The pole at ζ_0 yields the interesting part of the cochlea wave.

Then we use contour integration on the paths shown in Figure 5.5. For $X > 0$, the result is

$$\Phi(X, Y) = \frac{-i\Phi_0}{1 + i\omega\beta} e^{-i\zeta_0 X + \zeta_0 Y} + \frac{i\Phi_0}{1 + i\omega\beta} \frac{1}{2\pi} \int_0^\infty \left(\frac{e^{i\eta Y}}{i\eta - \zeta_0} + \frac{e^{-i\eta Y}}{i\eta + \zeta_0} \right) e^{-\eta X} \, d\eta \tag{26}$$

where the first term in (26) comes from the residue at the pole ζ_0. It should be noticed that this term by itself satisfies Laplace's equation and also the boundary condition on $Y = 0$, $X > 0$, but it fails to satisfy the condition on $X = 0$. Thus we can think of the integral in (26) as a correction that is needed to satisfy the latter boundary condition. This suggests that the solution for $\lambda a \neq \pi/2$ should have the same leading term with a more complicated integral correction.

Since we want to find the motion of the basilar membrane, we evaluate

$$\left.\frac{\partial \phi}{\partial y}\right|_{y=0} = \lambda e^{\lambda x}\left.\frac{\partial \Phi}{\partial Y}\right|_{Y=0} = \lambda\left(X\frac{\partial \Phi}{\partial Y}\right)\Bigg|_{Y=0}$$

$$= \frac{\lambda\zeta_0\Phi_0}{1+i\omega\beta}\left(-iXe^{-i\zeta_0 X} + \frac{1}{\pi}\int_0^\infty \frac{\eta X e^{-\eta X}\,d\eta}{\eta^2+\zeta_0^2}\right) \tag{27}$$

where $X = e^{\lambda x}$ since $y = 0$.

We shall study the two terms in (27) separately. First, let

$$\zeta_0 = \xi_0 - i\eta_0 \tag{28}$$

and consider

$$Xe^{-i\zeta_0 X} = \exp(\lambda x - i(\xi_0 - i\eta_0)e^{\lambda x})$$

$$= \exp(\lambda x - \eta_0 e^{\lambda x})\exp(-i\xi_0 e^{\lambda x}). \tag{29}$$

The amplitude in (29) has a maximum at x_p given by

$$1 = \eta_0 e^{\lambda x_p} \tag{30}$$

or

$$\lambda x_p = \log \eta_0^{-1}. \tag{31}$$

This suggests that we introduce the new variable $\tilde{x}$, defined by

$$x = x_p + \tilde{x}. \tag{32}$$

In terms of $\tilde{x}$, we can rewrite (29) as follows

$$X\exp(-i\zeta_0 X) = \eta_0^{-1}\exp(\lambda\tilde{x} - e^{\lambda\tilde{x}})\exp\left(-i(\xi_0/\eta_0)e^{\lambda\tilde{x}}\right). \tag{33}$$

We shall now obtain a bound on the integral that appears in (27). This bound holds when the dissipation is small in the sense that

$$\omega\beta < 1 \tag{34}$$

which implies $\mathrm{Re}(\zeta_0^2) > 0$. Let

$$I(X) = \frac{1}{\pi}\int_0^\infty \frac{\eta X e^{-\eta X}\,d\eta}{\eta^2+\zeta_0^2}. \tag{35}$$

Then

$$|I(X)| \leqslant \frac{1}{\pi}\int_0^\infty \frac{\eta X e^{-\eta X}\,d\eta}{|\zeta_0|^2} = \frac{1}{\pi|\zeta_0|^2 X} = \frac{\eta_0}{\pi|\zeta_0|^2}\,e^{-\lambda\tilde{x}} \tag{36}$$

where we have used $\eta_0 = e^{-\lambda x_p}$.

Combining these results and contemplating the limit $\eta_0 \to 0$ with $\tilde{x}$ fixed, we have the following formula for the velocity of the basilar membrane

$$v = \frac{-i\Phi_0}{1 + i\omega\beta} \frac{\zeta_0\lambda}{\eta_0} \exp\left\{\left(\lambda\tilde{x} - e^{\lambda\tilde{x}}\right)\right\} \exp\left\{ i\left(\omega t - \frac{\xi_0}{\eta_0} e^{\lambda\tilde{x}}\right)\right\} + O(\eta_0) \tag{37}$$

where $\tilde{x} = x - x_p$ and $\lambda x_p = \log(\eta_0^{-1})$.

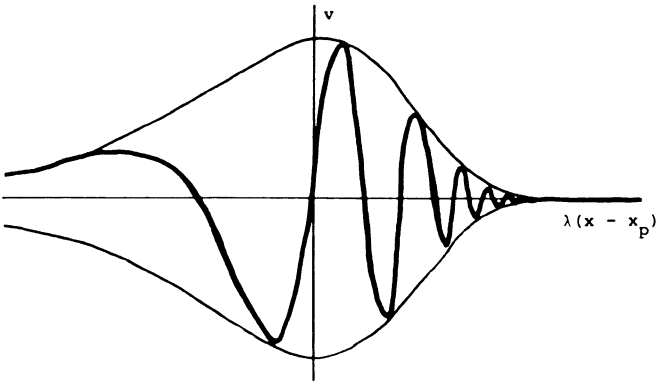

FIGURE 5.6. The cochlea wave and its envelope. The envelope rises like $\exp(\lambda(x - x_p))$ and decays like $\exp(-\exp(\lambda(x - x_p)))$.

Equation (37) describes a wave with an amplitude that rises exponentially for $\tilde{x}$ very negative and then decays like an exponential of an exponential for $\tilde{x}$ very positive. The phase of the wave increases exponentially with $\tilde{x}$. This result is plotted in Figure 5.6. As a function of $\tilde{x}$, the amplitude has a fixed form, independent of ω, but we still have to determine how x_p, the position of the peak, depends on ω.

From (25) and (28) we have, for $\omega\beta \ll 1$,

$$\xi_0 = \omega^2/\omega_0^2, \tag{38}$$

$$\eta_0 = \omega^3\beta/\omega_0^2 \tag{39}$$

and

$$-\lambda x_p = 3 \log(\omega/\omega_1) \tag{40}$$

where

$$\omega_1^3 = \omega_0^2/\beta. \tag{41}$$

Equation (40) gives the mapping from frequency to position that is established by the fluid dynamics of the cochlea in the inviscid case.

This relationship agrees with von Bekesy's measurements to the extent that the position of the peak is observed to vary as the negative logarithm of the frequency of the sound. According to (40) the dimensionless slope of this relationship ought to be 3, in different species this slope varies from about 1–3.

We have studied the form of the traveling wave as a function of position at fixed ω. Since each fiber of the auditory nerve has a particular value of x, it is also of interest to fix x and let ω vary In this way we can hope to find the frequency-response of the linear filter through which a given nerve fiber listens to the incident sound.

For this purpose, we start from (37), and we ignore the term $O(\eta_0)$. Also we assume that $\omega\beta \ll 1$ Let

$$A(x, \omega) = |v| = \frac{\Phi_0 \lambda \omega^2}{\omega_0^2} \frac{1}{\eta_0} \exp\{\lambda(x - x_p) - e^{\lambda(x - x_p)}\}$$

$$= \frac{\Phi_0 \lambda \omega^2}{\omega_0^2} \exp\left\{\lambda x - \frac{\omega^3 \beta}{\omega_0^2} e^{\lambda x}\right\} \tag{42}$$

where we have used $\eta_0 = e^{-\lambda x_p}$ As a function of ω, this has a maximum at $\omega = \omega_p(x)$ given by

$$2/3 = (\omega_p^3 \beta / \omega_0^2) e^{\lambda x} \tag{43}$$

so that

$$A(x, \omega_p) = (\Phi_0 \lambda \omega_p^2 / \omega_0^2) e^{\lambda x - 2/3} \tag{44}$$

and

$$\frac{A(x, \omega)}{A(x, \omega_p)} = \frac{\omega^2}{\omega_p^2} \exp\left\{\frac{2}{3} - \frac{\omega^3 \beta}{\omega_0^2} e^{\lambda x}\right\}$$

$$= \left(\frac{\omega}{\omega_p}\right)^2 \exp\left\{\frac{2}{3}\left(1 - \left(\frac{\omega}{\omega_p}\right)^3\right)\right\} \tag{45}$$

When describing filters, it is customary to plot $\log A$ against $\log \omega$. Accordingly, we evaluate

$$\log \frac{A(x, \omega)}{A(x, \omega_p)} = 2 \log \frac{\omega}{\omega_p} - \frac{2}{3}\left(\left(\frac{\omega}{\omega_p}\right)^3 - 1\right)$$

$$= 2 \log \frac{\omega}{\omega_p} - \frac{2}{3}\left(\exp\left\{3 \log \frac{\omega}{\omega_p}\right\} - 1\right) \tag{46}$$

which is plotted in Figure 5.7 Near $\omega = \omega_p$ we have

$$\log \frac{A(x, \omega)}{A(x, \omega_p)} \cong -3\left(\log \frac{\omega}{\omega_p}\right)^2 \tag{47}$$

so the tuning does not look particularly sharp near the peak. On the other hand, the cutoff on the high frequency side is, in a certain sense, arbitrarily sharp, since the slope on the right in Figure 5.7 is unbounded.

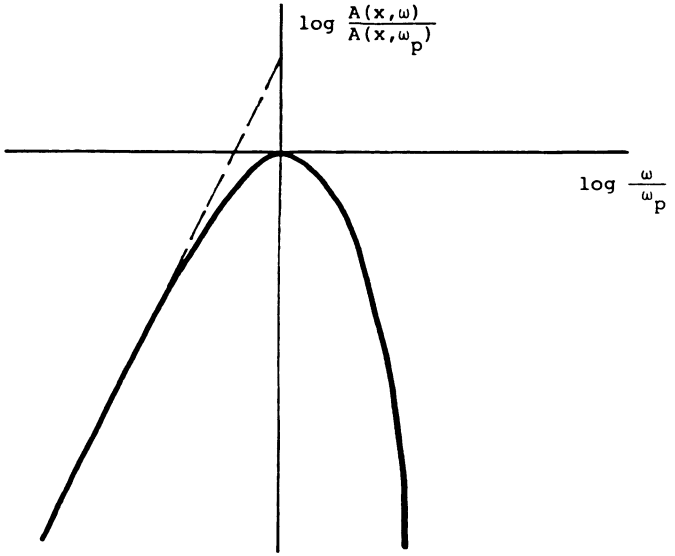

FIGURE 5.7. Amplitude vs. frequency at fixed x. The slope on the low frequency side approaches 2, but it approaches $-\infty$ on the high frequency side.

We conclude this section with some remarks concerning the importance of dissipation to the function of the cochlea. All of our results were obtained in the limit of low dissipation, so it might appear that we could dispense with friction altogether and set $\beta = 0$. The trouble with this can be seen immediately from the formula for x_p, equation (3), which shows that $x_p \to \infty$ as $\beta \to 0$. In fact, if we set $\beta = 0$, the interesting part of the solution is

$$v = -\frac{i\lambda\Phi_0\omega^2}{\omega_0^2} e^{\lambda x} \exp\left\{ i\left(\omega t - \frac{\omega^2}{\omega_0^2} e^{\lambda x}\right)\right\} \tag{48}$$

which is a wave with an amplitude and spatial frequency that both grow without bound as $x \to \infty$.

Thus, the fact that we get a peak at all is a consequence of the friction in the model. This does not mean that the friction has to be in the

basilar membrane, however In the next section we shall study the possibility that the dissipative mechanism of the cochlea is fluid viscosity

6. Numerical analysis of the cochlea with fluid viscosity. When $\mu \neq 0$, the method of analysis that we used in the previous section does not apply, and we have to make a fresh start beginning with equations (1)–(8) of the previous section. For simplicity, we shall assume that $\beta = 0$, but the corresponding equations for $\beta \neq 0$ can be found by substituting $s_0(1 + i\omega\beta)$ for s_0.

We shall start by reducing the equations of motion to an integral equation for the basilar membrane displacement. Then we shall describe two numerical methods for solving this integral equation.

First, look for solutions where

$$h(x, t) = H(x)e^{i\omega t} \tag{1}$$

and similarly for all of the other unknowns. Next take the Fourier transform with respect to x, so that

$$\hat{H}(\xi) = \frac{1}{\sqrt{2\pi}} \int_{-\infty}^{\infty} H(x)e^{-i\xi x}\, dx \tag{2}$$

and similarly for the other unknowns. The equations that result from these transformations are as follows. On $0 < |y| < a$·

$$i\omega\rho\hat{U} + i\xi\hat{P} = \mu(-\xi^2 + d^2/dy^2)\hat{U}, \tag{3}$$

$$i\omega\rho\hat{V} + d\hat{P}/dy = \mu(-\xi^2 + d^2/dy^2)\hat{V}, \tag{4}$$

$$i\xi\hat{U} + d\hat{V}/dy = 0. \tag{5}$$

On $y = \pm a$·

$$\hat{U} = \hat{V} = 0. \tag{6}$$

On $y = 0$:

$$\hat{U} = 0, \tag{7}$$

$$\hat{V} = i\omega\hat{H}, \tag{8}$$

$$[\hat{P}] = -s_0(e^{-\lambda x}H)\hat{} \tag{9}$$

The main complication here is in equation (9), where the explicit space dependence of the basilar membrane stiffness occurs. Equations (3)–(8) are a system of ordinary differential equations in y, which we can solve explicitly, in the sense that we can express $\hat{H}$ in terms of $[\hat{P}]$. We omit the details and just give the result:

$$\hat{H}(\xi) = -\hat{K}(\xi)[\hat{P}(\xi)] \tag{10}$$

where

$$\hat{K}(\xi) = \frac{1}{2}\,\frac{\xi}{\rho\omega^2\alpha}\,\frac{2\alpha\xi(1 - C_1C_2) + (\alpha^2 + \xi^2)S_1S_2}{\alpha C_1S_2 - \xi C_2S_1}, \tag{11}$$

$$C_1 = \cosh \xi a, \tag{12}$$

$$S_1 = \sinh \xi a, \tag{13}$$

$$C_2 = \cosh \alpha a, \tag{14}$$

$$S_2 = \sinh \alpha a, \tag{15}$$

$$\alpha = \sqrt{\xi^2 + i\omega\rho/\mu}\,. \tag{16}$$

When $a = \infty$, a case that is of interest because of the observation that the depth of the fluid can be increased without any change in the function of the cochlea, the expression for $\hat{K}$ simplifies as follows:

$$\hat{K}(\xi) = \frac{1}{2}\,\frac{|\xi|}{\rho\omega^2}\left(1 - \frac{1}{\sqrt{1 + i\omega\rho/\mu\xi^2}}\right) \tag{17}$$

which behaves like $|\xi|$ for small $|\xi|$ and like $|\xi|^{-1}$ for large $|\xi|$.

Substituting (9) in (10) we can eliminate $[\hat{P}]$ and obtain an equation for $\hat{H}$ alone:

$$\hat{H} = s_0\hat{K}(e^{-\lambda x}H)\hat{}\,. \tag{18}$$

There are two interesting ways to rewrite (18). First we can use the formal identity

$$(e^{-\lambda x}H)\hat{}\,(\xi) = \hat{H}(\xi - \lambda i) \tag{19}$$

to obtain the functional equation

$$\hat{H}(\xi) = s_0\hat{K}(\xi)\hat{H}(\xi - \lambda i). \tag{20}$$

Alternatively, we can introduce the operator notation

F = Fourier transform ($F^* = F^{-1}$),

$\hat{K}$ = multiplication by $\hat{K}(\xi)$,

E = multiplication by $e^{-\lambda x}$.

Applying F^* to (18), we get

$$H = s_0F^*\hat{K}FEH \tag{21}$$

which is an integral equation, since $F^*\hat{K}F$ corresponds to convolution with the function $K = F^*\hat{K}$.

Equation (21) has the form of an eigenproblem for the operator $F^*\hat{K}FE$, which is not selfadjoint. The eigenvalue s_0^{-1} is given, but its value plays no essential role. To see this, let T_b be the translation operator

$$(T_bH)(x) = H(x - b). \tag{22}$$

Note that T_b commutes with $F^*\hat{K}F$, but

$$(T_bEH)(x) = e^{-\lambda(x-b)}H(x-b) = e^{\lambda b}(ET_bH)(x). \tag{23}$$

Applying T_b to (21), we get

$$(T_bH) = s_0e^{\lambda b}F^*\hat{K}FE(T_bH). \tag{24}$$

In summary, if H is a solution to (21) corresponding to s_0, then $H_b = T_bH$ is a solution corresponding to $s_b = s_0e^{\lambda b}$. Since b can be any real number, s_0 can be replaced by any positive number without any essential change in the problem. In the following we set $s_0 = 1$

The problems (20) and (21) can be restated in least-squares form. Minimize

$$Q = \|\hat{A}\hat{H}\|/\|\hat{H}\| = \|AH\|/\|H\| \tag{25}$$

where

$$A = I - F^*\hat{K}FE, \tag{26}$$

$$\hat{A} = FAF^* = I - \hat{K}FEF^* \tag{27}$$

and where $\|\ \|$ is the L_2-norm

$$\|H\|^2 = \int_{-\infty}^{\infty} |H(x)|^2\,dx. \tag{28}$$

The two forms of Q in (25) are equal because F preserves the L_2-norm.

The advantage of this formulation is that it survives discretization. In the continuous context, the operator $F^*\hat{K}FE$ has a continuous spectrum, so we were free to fix $s_0 = 1$ In the discrete context with N degrees of freedom, such an arbitrary choice of s_0 is very likely to lead to nonexistence of the solution, since there is no longer any reason for 1 to be an eigenvalue. With the least-squares formulation, we can still try to minimize Q For each N, we expect $Q_{\min} > 0$, but we also expect to find that $Q_{\min} \to 0$ as $N \to \infty$

Any method for discretizing (25) will lead to the problem of minimizing a Rayleigh quotient

$$Q^2 = w^*Mw/w^*w \tag{29}$$

where w is a vector that represents H, M is a nonnegative Hermitian matrix corresponding to A^*A, and * stands for Hermitian conjugation.

The minimization can be carried out by means of the inverse power method, which is an iteration in which w^{n+1} is found from w^n by solving

$$Mw^{n+1} = w^n/\|w^n\| \tag{30}$$

Let V_0 be the space of vectors that minimize Q This is the eigenspace corresponding to the smallest eigenvalue of M Then w^n converges

towards some vector w in V_0 as $n \to \infty$ unless the initial guess is orthogonal to V_0. This exceptional case can be avoided by choosing the components of the initial guess with a random number generator. Moreover, once convergence has been obtained, we have

$$Mw = w/\|w\| \tag{31}$$

so

$$Q_{\min} = w^* Mw/w^* w = 1/\|w\|. \tag{32}$$

It has been proved by Wilkinson that the effectiveness of the inverse power method is *not* destroyed by roundoff error when M is nearly singular.

We shall now describe two methods of discretizing the least-squares problem (25). The first method was used by the present author and the second was used by Eli Isaacson.

In the first method, we introduce a mesh of N equally spaced points on the x-axis, and a corresponding mesh on the ξ-axis. The mesh-widths are chosen as

$$\lambda \Delta x_N = \Delta \xi_N / \lambda = (2\pi/N)^{1/2} \tag{33}$$

and the mesh points are given by

$$x_j^N = j\Delta x, \tag{34}$$

$$\xi_k^N = k\Delta\xi \tag{35}$$

where $j, k = -N/2, \ldots, N/2 - 1$. As N is increased these meshes get finer, but they also cover more of the x- and ξ-axes. For example, when N is replaced by $4N$, each mesh gets twice as fine and twice as long.

Discretization of the Fourier transform in these meshes gives the equations

$$\begin{aligned} \hat{H}_N(\xi_k^N) &= \left(\frac{1}{2\pi}\right)^{1/2} \sum_j H_N(x_j^N) \exp(-i\xi_k^N x_j^N) \Delta x_N \\ &= \frac{1}{\lambda} \frac{1}{N^{1/2}} \sum_j H_N(x_j^N) \exp(-i(2\pi/N)jk), \end{aligned} \tag{36}$$

$$\begin{aligned} H_N(x_j^N) &= \left(\frac{1}{2\pi}\right)^{1/2} \sum_k \hat{H}_N(\xi_k^N) \exp(i\xi_k^N x_j^N) \Delta\xi_N \\ &= \lambda \frac{1}{N^{1/2}} \sum_k \hat{H}_N(\xi_k^N) \exp(i(2\pi/N)jk) \end{aligned} \tag{37}$$

which may be summarized

$$\hat{H}_N = F_N H_N/\lambda, \tag{38}$$

$$H_N = \lambda F_N^* \hat{H}_N \tag{39}$$

where F_N is the discrete Fourier transform, which is defined as

$$(F_N)_{jk} = \frac{1}{N^{1/2}} e^{-i(2\pi/N)jk} \tag{40}$$

Using the formula for the sum of a geometric series, one can show that

$$F_N^* F_N = I \tag{41}$$

which proves that (38) and (39) are consistent with each other

The multiplication operators E and $\hat{K}$ that appear in (25)–(27) are represented by diagonal matrices

$$E_N = \text{diag}(\ .\ .\ \ e^{-\lambda x_j^N}\ \ \ ), \tag{42}$$

$$\hat{K}_N = \text{diag}(\ \ .\ \ \hat{K}(\xi_k^N)\ \ \ ) \tag{43}$$

and we use the discrete L_2-norms defined by

$$\|H_N\|^2 = \sum_j |H_N(x_j^N)|^2 \Delta x_N = \frac{1}{\lambda}\left(\frac{2\pi}{N}\right)^{1/2} \sum_j |H_N(x_j^N)|^2, \tag{44}$$

$$\|\hat{H}_N\|^2 = \sum_k |\hat{H}_N(\xi_k^N)|^2 \Delta\xi_N = \lambda\left(\frac{2\pi}{N}\right)^{1/2} \sum_k |\hat{H}_N(\xi_k^N)|^2. \tag{45}$$

These expressions are normalized in such a way that they converge to the square of the L_2-norm as $N \to \infty$. Moreover, we have $\|H_N\| = \|\hat{H}_N\|$ when H_N and $\hat{H}_N$ are related as in (38)–(39).

Finally we need an operator "inter" that will take a mesh function on the mesh of order $N/4$ and construct a corresponding function on the mesh of order N This operator will be defined by trigonometric interpolation to the interior mesh points with extension by zero to the exterior mesh points. Note that inter preserves the norms we have introduced above.

The discrete Rayleigh quotient is

$$Q_N^2 = \frac{H_N^* A_N^* A_N H_N}{H_N^* H_N} \tag{46}$$

We combine the inverse power method with the process of letting $N \to \infty$ by performing one inverse power step on each mesh and then transferring the solution to a mesh which has four times as many points (twice as fine and twice as long). This may be written

$$A_N^* A_N H_N = B_N \tag{47}$$

where

$$B_N = \text{inter}(H_{N/4}/\|H_{N/4}\|). \tag{48}$$

To measure how much the solution has changed at each step, we use the parameter θ_N defined by

$$\cos^2 \theta_N = |H_N^* B_N|^2 / (H_N^* H_N)(B_N^* B_N). \tag{49}$$

Also, to measure how close we have come to solving the original problem we use

$$\|H_N\| = 1/Q_N(H_N). \tag{50}$$

Numerical evidence that the computed H_N is converging to a solution of the continuous problem would be $\theta_N \to 0$ and $\|H_N\| \to \infty$ as $N \to \infty$. Such results are shown in Table 1.

TABLE 1. Numerical evidence for convergence.

N	$\|H_N\|$	θ_N
64	2.45	1.32
256	473.	0.472
1024	712.	0.057

N	$\|H_N\|$	θ_N
128	4.89	1.36
512	615.	0.227
2048	782.	0.035

We still have to explain how the linear system (47) is solved. First, we scale the problem in the following way. Let

$$H_N = D_N G_N \tag{51}$$

and multiply by D_N to obtain

$$D_N A_N^* A_N D_N G_N = D_N B_N. \tag{52}$$

We choose D_N as a diagonal matrix, with diagonal elements chosen in such a way that

$$(D_N A_N^* A_N D_N)_{jj} = 1. \tag{53}$$

It follows from the Schwartz inequality that all of the off-diagonal elements of the scaled matrix are bounded by 1 in absolute value.

Note that this scaling procedure is only a means towards solving (47). In particular, we are applying the inverse power method to the original matrix $A_N^* A_N$, not to the scaled matrix $D_N A_N^* A_N D_N$. This is important, since the latter matrix has a different spectrum.

The choice of a method for solving the scaled problem (52) is dictated by the following considerations. The matrix that appears in (52) is a large, symmetric positive definite matrix. It is *not* a sparse matrix, but it has in common with sparse matrices the property that it can be

multiplied by an arbitrary vector very efficiently The reason for this is that the required operations involve multiplication by diagonal matrices and fast Fourier transform operations.

The *conjugate gradient method* for solving symmetric, positive definite systems has the property that it uses the matrix of the system only in the form of a subroutine that can multiply this matrix by an arbitrary vector In our case this can be done very efficiently (without ever storing the matrix) for the reason that was given above. Accordingly, this is the method of choice. In practice, we use the subroutine package SYMMLQ, which is a more general form of the conjugate gradient method than we require here, since it can also handle the indefinite case.

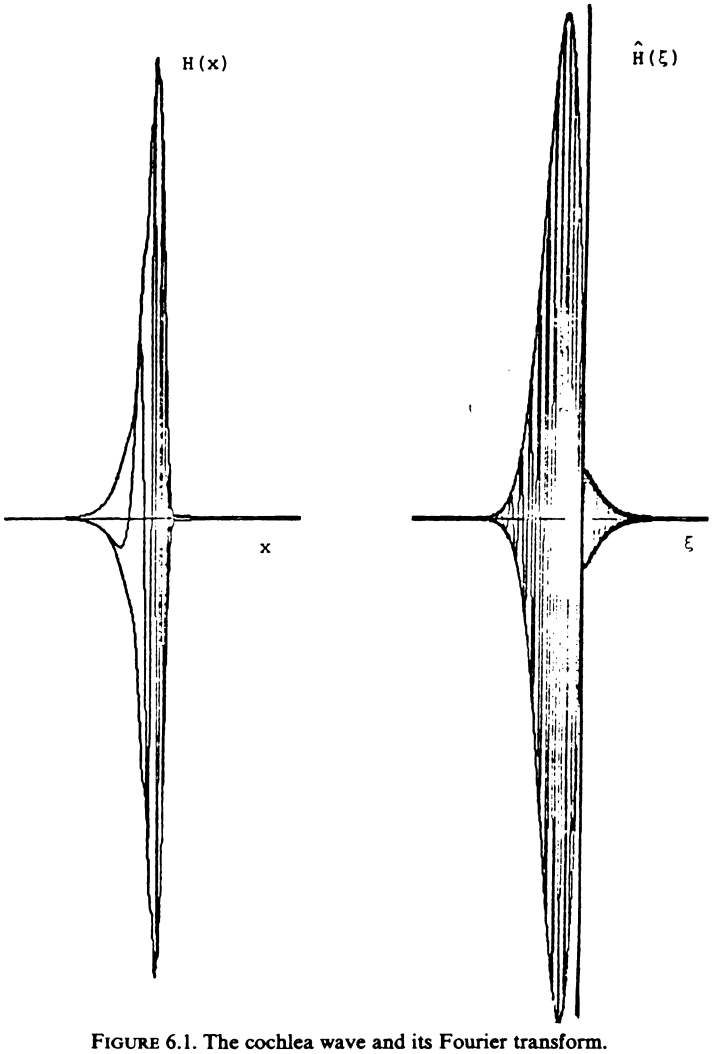

FIGURE 6.1. The cochlea wave and its Fourier transform.

The method that we have just described was used to compute the response of the basilar membrane to a pure tone when fluid viscosity is the dissipative mechanism. The basilar membrane displacement H and its Fourier transform $\hat{H}$ are plotted in Figure 6.1. Note that the qualitative features are the same as in the previous section where basilar membrane friction was the dissipative mechanism.

The fact that the Fourier transform shows predominantly negative frequencies means that the wave is propagating into the cochlea in the direction of increasing x. This is a remarkable result when we consider that the computational method makes no explicit reference to a source. Thus the direction of propagation is determined by the gradient of compliance along the basilar membrane, since this is the only feature of the model that distinguishes increasing x from decreasing x. This is consistent with von Bekesy's observations on paradoxical waves that was mentioned in the previous section.

Let us now consider a completely different method for discretizing the least-squares problem (25). This method was introduced by Eli Isaacson; it is an example of the Rayleigh-Ritz procedure of minimizing over a subspace.

In Isaacson's method, we minimize the Rayleigh quotient Q over the subspace of L_2 that is spanned by the first N Hermite functions. These are the functions that are formed by applying the Gram-Schmidt procedure to the sequence

$$e^{-x^2/2},\ xe^{-x^2/2},\ x^2e^{-x^2/2},\ \ldots. \tag{54}$$

That is

$$\phi_n(x) = p_n(x)e^{-x^2/2} \tag{55}$$

where $p_n(x)$ is a polynomial of degree n chosen so that

$$\int_{-\infty}^{\infty} \phi_n(x)\phi_m(x)\,dx = \begin{cases} 1, & n = m, \\ 0, & n \neq m. \end{cases} \tag{56}$$

Note that the Fourier transform of $e^{-x^2/2}$ is $e^{-\xi^2/2}$. More generally, the Hermite functions are eigenfunctions of the Fourier transformation with eigenvalues that are ± 1 or $\pm i$.

The procedure is to write

$$\hat{H}_N(\xi) = \sum_{k=0}^{N} c_k \hat{\phi}_k(\xi) \tag{57}$$

and then choose c_k to minimize

$$Q^2 = \frac{\int_{-\infty}^{\infty} |\hat{H}_N(\xi) - \hat{K}(\xi)\hat{H}_N(\xi - \lambda i)|^2\,d\xi}{\int_{-\infty}^{\infty} |\hat{H}_N(\xi)|^2\,d\xi} \tag{58}$$

$$= \frac{\sum_{j=0}^{N}\sum_{k=0}^{N} \bar{c}_j c_k M_{jk}}{\sum_{k=0}^{N} |c_k|^2} \tag{59}$$

where

$$M_{jk} = \int_{-\infty}^{\infty} \overline{\left(\hat{\phi}_j(\xi) - \hat{K}(\xi)\hat{\phi}_j(\xi - \lambda i)\right)} \left(\hat{\phi}_k(\xi) - \hat{K}(\xi)\hat{\phi}_k(\xi - \lambda i)\right) d\xi. \tag{60}$$

Fortunately the functions $\hat{\phi}_k$ are entire functions, so the expressions $\hat{\phi}_k(\xi - \lambda i)$ always make sense.

Note that the formula for M_{jk} does not involve N. This is convenient, because it means that when N is increased, we just have to compute more matrix elements, but we do not have to recompute the old ones. Isaacson uses Gauss-Hermite quadrature to evaluate the matrix elements M_{jk}.

The minimization of (59) is carried out by the inverse power method, as before, but the linear systems are solved by Cholesky factorization. Again, when N is increased one can take advantage of the part of the Cholesky factorization that has already been carried out.

Isaacson applied this method to a cochlea model with a realistic finite depth and obtained results for a wide range of frequencies. Figure 6.2 shows his plot of the position of the peak as a function of the log of the frequency. The linearity of this plot is remarkable.

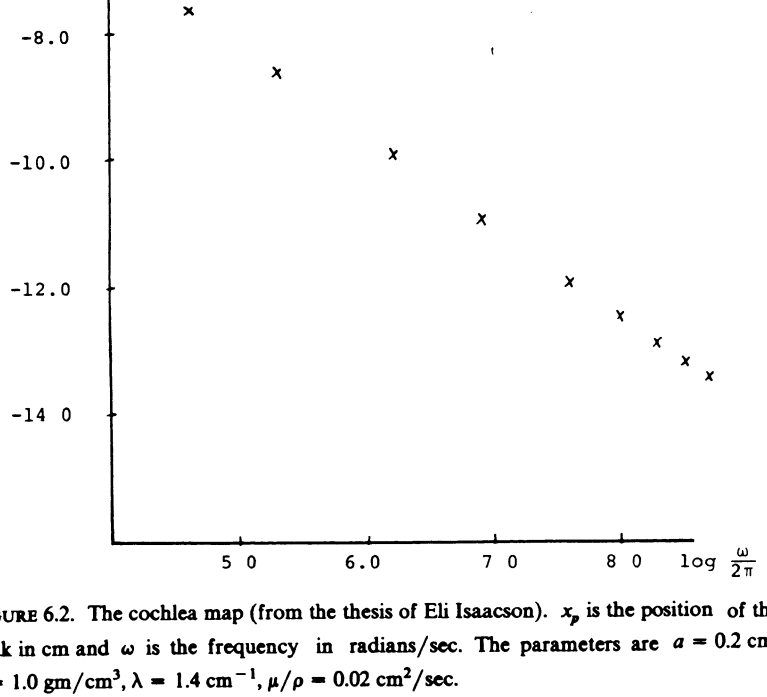

FIGURE 6.2. The cochlea map (from the thesis of Eli Isaacson). x_p is the position of the peak in cm and ω is the frequency in radians/sec. The parameters are $a = 0.2$ cm, $\rho = 1.0$ gm/cm^3, $\lambda = 1.4$ cm^{-1}, $\mu/\rho = 0.02$ cm^2/sec.

7. The stochastic auditory code. The motion of the basilar membrane at any point has to be coded as a train of nerve impluses before it can be transmitted to the brain. A surprising fact about this code is that it is not deterministic. The pattern of impulses on the fibers of the auditory nerve was studied by Kiang, who found that the response of a given fiber to a click was not reproducible from one presentation of the click to the next.

After many presentations of the same stimulus, the statistical pattern becomes clear, however It can be summarized by saying that the probability per unit time that a nerve impulse will be generated depends on the instantaneous displacement of the basilar membrane. There is often a spontaneous rate of firing, and displacement of the basilar membrane in one direction increases the rate while displacement in the other direction decreases it. In some cases the spontaneous rate is essentially zero, so that only displacements in one direction have any effect.

In this section, we shall present a formal model that was proposed by Gestri to account for this sort of coding. (A similar model was introduced by Bruce Knight at the same time, but our analysis follows Gestri's more closely.) The model contains a stochastic threshold, and it has the beautiful feature that many of the key properties of the model are independent of the choice of the threshold distribution.

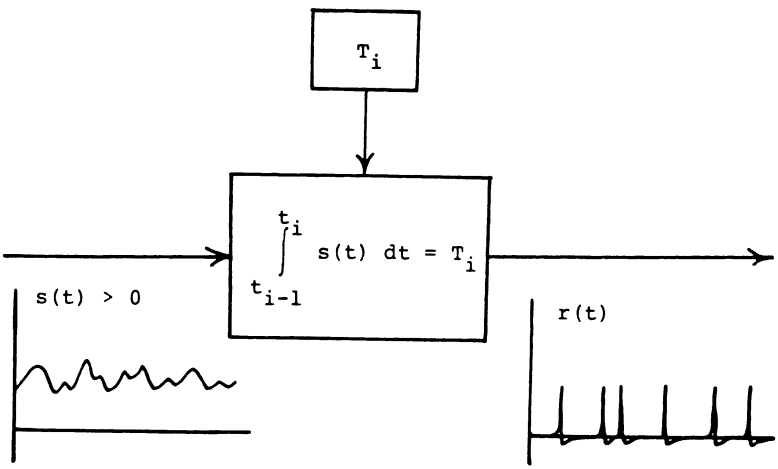

FIGURE 7.1. Gestri's model for a stochastic encoding neuron. The input is a positive signal $s(t)$ and the output is a sequence of nerve impulses at time t_i. The thresholds, T_i, are chosen at random.

Gestri's model is shown in Figure 7 1 The input to the model is a signal $s(t)$ which is assumed to be positive. The output is a sequence of times t_i at which nerve impulses are generated. It will also be convenient

to think of the output in terms of the idealized neural response:

$$r(t) = \sum_{i=0}^{\infty} \delta(t - t_i). \tag{1}$$

The random elements of the model are the thresholds T_i which are positive, independent, random variables which all have the same probability density function $f(T)$. The firing times t_i are defined recursively by the equation

$$\int_{t_{i-1}}^{t_i} s(t)\, dt = T_i, \qquad i = 1, 2, \ldots. \tag{2}$$

The method for choosing the random variable t_0 will be specified below.

The physical picture that leads to this formal model is as follows. Somehow, basilar membrane displacement is converted into an electric current that charges up the nerve cell membrane, which acts like a capacitor This charging process explains the integration in (2) since charge is the integral of current. As is well known, nerve membranes behave in a highly nonlinear way, and they fire an impulse when a certain threshold is reached. A possible interpretation of the random behavior of the auditory nerve is that the threshold is fluctuating. Gestri models this fluctuation by assuming a threshold which is chosen anew after each nerve impulse and then held constant until the next nerve impulse.

This model is highly idealized in several respects. In particular, it is important to point out that real cell membranes are leaky so that the charge is not quite the integral of the stimulus current. Bruce Knight and Richard Stein have shown that this leakiness leads to some very interesting effects in neurons with a fixed threshold. In particular, a population of such neurons can be synchronized by a periodic stimulus. Knight and Stein have also shown that randomness of the threshold combats this tendency to synchronization. These results suggest that the pure integrate-and-fire model is only adequate when the threshold is sufficiently random.

The analysis of Gestri's model is greatly simplified by introducing the transformed time

$$S(t) = \int_0^t s(t')\, dt' \tag{3}$$

and writing $S_i = S(t_i)$ for the firing times expressed in terms of S Then (2) becomes

$$S_i - S_{i-1} = T_i, \qquad i = 1, 2, \tag{4}$$

Note that the statistics of S_i are completely independent of the signal $s(t)$, which only comes in when we transform back to t_i.

Let $\rho_i(S)$ be the probability density function for S_i. Then

$$\rho_i(S) = \int_0^S \rho_{i-1}(S - T)f(T)\,dT \tag{5}$$

or

$$\rho_i = \rho_{i-1} * f \tag{6}$$

where $*$ is the convolution that is defined in (5).

We still have to choose $\rho_0(S)$. This will be done in such a way that

$$\sum_{i=0}^{\infty} \rho_i(S) = R, \quad \text{independent of } S. \tag{7}$$

This choice effectively hides the origin $t = 0$ ($S = 0$) so that the process looks as if it has been running forever. An explicit formula for ρ_0 can be found as follows. Apply $f *$ to both sides of (7):

$$f * R = \sum_{i=0}^{\infty} f * \rho_i = \sum_{i=1}^{\infty} \rho_i = R - \rho_0. \tag{8}$$

Thus

$$\rho_0 = R - f * R = R(1 - f * 1) \tag{9}$$

or

$$\rho_0(S) = R\left(1 - \int_0^S f(T)\,dT\right). \tag{10}$$

The constant R is not arbitrary; it can be found from the condition

$$\begin{aligned} 1 &= \int_0^{\infty} \rho_0(S)\,dS = R\int_0^{\infty}\left(1 - \int_0^S f(T)\,dT\right)dS \\ &= R\int_0^{\infty} f(S)S\,dS = RE[T_i] \end{aligned} \tag{11}$$

where $E[\ ]$ stands for expected value. Thus R is the reciprocal of the expected value of the threshold. It is the expected rate of nerve impulses when $s(t) = 1$.

To get an intuitive feel for the choice of ρ_0 that we have made, it is instructive to consider the special case

$$f(T) = \delta(T - T_0) \tag{12}$$

in which the threshold has the fixed value T_0 and $R = 1/T_0$. According to (10)

$$\rho_0(S) = \begin{cases} 1/T_0, & 0 < S < T_0, \\ 0, & S > T_0. \end{cases} \tag{13}$$

In other words, S_0 is uniformly distributed on the interval $(0, T_0)$. Thus the deterministic threshold is a special case, and the model is still

stochastic in this case because S_0 is a random variable. This randomness in the 0th firing time comes about because the initial value assigned to the integrator is a random variable.

We now consider the distributions of the firing times t_i. Let $\sigma_i(t)$ be the probability density function for t_i. Then

$$\sigma_i(t)dt = \rho_i(S(t))dS, \tag{14}$$

$$\sigma_i(t) = \rho_i(S(t))s(t) \tag{15}$$

where we have used $s(t) = dS/dt$, which follows from (3). If we sum (15) over all i, we obtain

$$\sigma(t) = \sum_{i=0}^{\infty} \sigma_i(t) = Rs(t). \tag{16}$$

This shows that the expected density of nerve impulses is proportional to the signal $s(t)$. Note that this result holds for all threshold distributions!

We can express the same result in another way by regarding the output of our system as the response function $r(t)$ given by equation (1). Then

$$E[r(t)] = \sum_{i=0}^{\infty} \int_0^{\infty} \delta(t - t')\sigma_i(t')\, dt'$$

$$= \sum_{i=0}^{\infty} \sigma_i(t) = Rs(t). \tag{17}$$

Thus the expected value of the output is proportional to the input.

It is often useful to regard the signal $s(t)$ as a sample of a stationary stochastic process with mean

$$s_0 = E[s(t)] \tag{18}$$

and with autocorrelation function

$$\phi_{ss}(b - a) = E[(s(b) \quad s_0)(s(a) - s_0)] \tag{19}$$

The power spectrum of the signal is the Fourier transform of its autocorrelation function.

$$\hat{\phi}_{ss}(\omega) = \int_{-\infty}^{\infty} \phi_{ss}(\tau)e^{-i\omega\tau}\, d\tau \tag{20}$$

The name "power spectrum" comes from the formula

$$E[(s(t) - s_0)^2] = \phi_{ss}(0) = \frac{1}{2\pi}\int_{-\infty}^{\infty} \hat{\phi}_{ss}(\omega)\, d\omega. \tag{21}$$

In many applications the first expression in (21) is proportional to the average instantaneous power and the last expression shows that $(1/2\pi)\hat{\phi}_{ss}(\omega)$ is the density of the power with respect to frequency

When $s(t)$ is a stationary stochastic process, so is $r(t)$, and we shall see how its statistical properties are related to those of s. From (17) we can calculate the mean value of r and also the cross-correlation of r and s:

$$r_0 = E[r(t)] = RE[s(t)] = Rs_0, \tag{22}$$

$$\begin{aligned}\phi_{rs}(b-a) &= E[(r(b)-r_0)(s(a)-s_0)] \\ &= RE[(s(b)-s_0)(s(a)-s_0)] \\ &= R\phi_{ss}(b-a).\end{aligned} \tag{23}$$

Again, these simple results are independent of the form of the threshold distribution.

Something much more complicated happens, though, when we try to calculate the autocorrelation function ϕ_{rr} and the output power spectrum $\hat{\phi}_{rr}$. We have

$$\begin{aligned}\phi_{rr}(b-a) &= E[(r(b)-r_0)(r(a)-r_0)] \\ &= E[r(b)r(a)] - r_0^2 \\ &= E\left[\sum_{j=0}^{\infty}\delta(b-t_j)\sum_{i=0}^{\infty}\delta(a-t_i)\right] - r_0^2.\end{aligned} \tag{24}$$

To proceed further we need to introduce the joint density $\sigma_{ij}(\ ,\ )$ for the firing times t_i, t_j and also the corresponding density $\rho_{ij}(\ ,\ )$ for the S-values of these firing times S_i and S_j. These joint densities are related by

$$\sigma_{ij}(a, b) = \rho_{ij}(S(a), S(b))s(a)s(b) \tag{25}$$

which is analogous to (15). Moreover, $\sigma_{ij}(a, b) = 0$ unless the signs of $(b-a)$ and $(j-i)$ are the same. When $b > a$ and $j > i$, we have

$$\sigma_{ij}(a, b) = \rho_i(S(a))f_{j-i}(S(b) - S(a))s(a)s(b) \tag{26}$$

where we have introduced the functions f_k defined by

$$f_1 = f, \tag{27}$$

$$f_k = f * f_{k-1}, \qquad k = 2, 3, \ldots. \tag{28}$$

It will also be useful to introduce

$$F = \sum_{k=1}^{\infty} f_k. \tag{29}$$

With this notation, we have, for $b > a$,

$$\sum_{i=0}^{\infty}\sum_{j=i+1}^{\infty}\sigma_{ij}(a, b) = RF(S(b) - S(a))s(a)s(b). \tag{30}$$

We are now ready to complete the evaluation of (24). The procedure is to take the expectation over all choices of the thresholds T_i with $s(t)$

fixed and then take the expectation over all choices of $s(t)$:

$$\begin{aligned}\phi_{rr}(b-a) &= E\Bigg[\sum_{i=0}^{\infty}\sum_{j=i+1}^{\infty}\int_0^\infty\int_0^\infty \delta(b-t'')\delta(a-t')\sigma_{ij}(t',t'')\,dt'\,dt'' \\ &\qquad + \sum_{i=0}^{\infty}\int_0^\infty \delta(b-t')\delta(a-t')\sigma_i(t')\,dt'\Bigg] - r_0^2 \\ &= E\Bigg[\sum_{i=0}^{\infty}\sum_{j=i+1}^{\infty}\sigma_{ij}(a,b) + \sum_{i=0}^{\infty}\sigma_i(a)\delta(b-a)\Bigg] - r_0^2 \\ &= E\big[RF(S(b)-S(a))s(a)s(b) + Rs(t)\delta(b-a)\big] - r_0^2 \\ &= E\big[RF(S(b)-S(a))s(a)s(b)\big] + Rs_0\delta(b-a) - R^2s_0^2. \end{aligned} \tag{31}$$

It is convenient to split F into $R + (F - R)$. This gives

$$\begin{aligned}\phi_{rr}(b-a) &= R^2\phi_{ss}(b-a) + Rs_0\delta(b-a) \\ &\qquad + E\big[R(F(|S(b)-S(a)|)-R)s(a)s(b)\big]\end{aligned} \tag{32}$$

where we have inserted the absolute value sign to make (32) valid for $b < a$ as well as $b > a$.

An important special case is $F(S) = R$ for all $S > 0$. This comes about when $f(T) = Re^{-RT}$ so that the output of Gestri's model reduces to a modulated Poisson process. In this case the correlation function is simply

$$\phi_{rr}(\tau) = R^2\phi_{ss}(\tau) + Rs_0\delta(\tau) \tag{33}$$

and the power spectrum is

$$\hat{\phi}_{rr}(\omega) = R^2\hat{\phi}_{ss}(\omega) + Rs_0. \tag{34}$$

Recalling the form of the cross-correlation, equation (23), we see that as far as the correlation functions are concerned, the situation is the same as if we had put the signal through an amplifier with gain R and then added uncorrelated white noise with spectral density Rs_0.

In general, it seems difficult to evaluate the power spectrum corresponding to (32). Just to take the expected value of the last term in (32) requires knowledge of the joint distribution of $s(a)$, $s(b)$, and $\int_a^b s(t)\,dt$ This means that we have to know more about s than just its correlation function ϕ_{ss}. We can, however, examine the correlation function ϕ_{rr}^0 which results from setting $s = s_0$ (no signal). This gives an indication of the noise that is introduced by the encoding neuron. We have

$$\begin{aligned}\phi_{rr}^0(\tau) &= Rs_0\delta(\tau) + R(F(s_0|\tau|) - R)s_0^2 \\ &= Rs_0(\delta(\tau) + s_0(F(s_0|\tau|) - R)).\end{aligned} \tag{35}$$

To get the power spectrum, we have to take the Fourier transform of (35). First note that the transform of (29) is

$$\hat{F}(\omega) = \sum_{k=1}^{\infty} (\hat{f}(\omega))^k = \frac{\hat{f}(\omega)}{1 - \hat{f}(\omega)} \tag{36}$$

which has a simple pole at $\omega = 0$, since

$$\hat{f}(0) = \int_0^{\infty} f(T)\, dT = 1 \tag{37}$$

and

$$\hat{f}'(0) = -i \int_0^{\infty} Tf(T)\, dT = -i/R. \tag{38}$$

Using these results we can show that $F(S) \to R$ as $S \to \infty$. The function

$$G(\tau) = s_0(F(s_0|\tau|) - R) \tag{39}$$

has

$$\hat{G}(\omega) = 2 \text{ Re } \frac{\hat{f}(\omega/s_0)}{1 - \hat{f}(\omega/s_0)}. \tag{40}$$

We can now take the Fourier transform of (35) and obtain

$$\hat{\phi}_{rr}^0(\omega) = Rs_0\left(1 + 2 \text{ Re } \frac{\hat{f}(\omega/s_0)}{1 - \hat{f}(\omega/s_0)}\right) \tag{41}$$

for the spectrum of the neural response in the absence of signal.

This suggests the following design problem. Choose $f(T)$ to minimize

$$M = \sup_{\omega} \hat{\phi}_{rr}^0(\omega) \tag{42}$$

subject to the constraints

$$\int_0^{\infty} f(T)\, dT = 1, \tag{43}$$

$$\int_0^{\infty} Tf(T)\, dT = 1/R, \tag{44}$$

$$\lim_{\omega \to \infty} \hat{f}(\omega) = 0. \tag{45}$$

Equation (45) is a regularity condition. Although it appears to rule out the interesting case in which $f(T) = \delta(T - T_0)$, we shall study this as a limiting case below From (45), we conclude that

$$M > Rs_0. \tag{46}$$

Accordingly, a threshold density f is *optimal* (solves the design problem) if it satisfies

$$\operatorname{Re} \frac{\hat{f}(\omega)}{1 - \hat{f}(\omega)} \leqslant 0, \quad \text{all } \omega \tag{47}$$

since such threshold densities have $M = Rs_0$.

We shall look for optimal threshold densities among a particular class of functions defined by

$$\hat{f}^{(n)}(\omega) = \frac{1}{(1 + i\omega/nR)^n} \tag{48}$$

We leave it to the reader to verify that the constraints are satisfied and that

$$f^{(1)}(T) = \begin{cases} Re^{-RT}, & T > 0, \\ 0, & T < 0, \end{cases} \tag{49}$$

while

$$\lim_{n \to \infty} f^{(n)}(T) = \delta(T - 1/R). \tag{50}$$

Thus at $n = 1$, we have the threshold density that generates a Poisson process of firing times. As $n \to \infty$, we approach the deterministic threshold distribution.

We shall now determine the set of values of n for which (47) holds. We have

$$\frac{\hat{f}^{(n)}(\omega)}{1 - \hat{f}^n(\omega)} = \frac{1}{(1 + i\omega/nR)^n - 1}, \tag{51}$$

$$\begin{aligned} 2 \operatorname{Re} \frac{\hat{f}^{(n)}(\omega)}{1 - \hat{f}^n(\omega)} &= \frac{1}{(1 + i\omega/nR)^n - 1} + \frac{1}{(1 - i\omega/nR)^n - 1} \\ &= \frac{(1 + i\omega/nR)^n + (1 - i\omega/nR)^n - 2}{|(1 + i\omega/nR)^n - 1|^2} \end{aligned} \tag{52}$$

The denominator in (52) is positive unless $\omega = 0$. The limiting value of (52) as $\omega \to 0$ is

$$\frac{-2\binom{n}{2}\omega^2/n^2R^2}{\omega^2/R^2} = -\frac{n(n-1)}{n^2} = -\left(1 - \frac{1}{n}\right) < 0. \tag{53}$$

For $\omega \neq 0$, we only need to look at the sign of the numerator in (52). We write out the numerator for the cases $n = 1$, 2, 3, and 4:

$$N_1 = 0, \tag{54}$$

$$N_2 = -2\omega^2/n^2R^2, \tag{55}$$

$$N_3 = -6\omega^2/n^2R^2, \tag{56}$$

$$N_4 = -12\omega^2/n^2R^2 + 2\omega^4/n^4R^4 \tag{57}$$

Clearly N_1, N_2, and N_3 are nonpositive, but N_4 is positive for ω sufficiently large. Thus (47) holds for $n = 1, 2, 3$ but not for $n = 4$. We can also show that it fails for $n > 4$, by considering the special value of ω given by

$$\omega_0/nR = \tan(2\pi/n) \tag{58}$$

so that

$$1 + i\omega_0/nR = e^{i2\pi/n}/\cos(2\pi/n). \tag{59}$$

When $n > 4$, $0 < \cos(2\pi/n) < 1$ This gives

$$\left(1 + i\frac{\omega_0}{nR}\right)^n = \left(1 - i\frac{\omega_0}{nR}\right)^n = \frac{1}{(\cos(2\pi/n))^n} > 1 \tag{60}$$

It follows that (47) is false for $n > 4$. Moreover,

$$\left(1 + i\frac{\omega_0}{nR}\right)^n \sim \frac{1}{\left(1 - \frac{1}{2}(2\pi/n)^2\right)^n} \sim 1 + \frac{n}{2}\left(\frac{2\pi}{n}\right)^2 = 1 + \frac{2\pi^2}{n} \tag{61}$$

Substituting in (51), we see that

$$\frac{\hat{f}^{(n)}(\omega_0)}{1 - \hat{f}^{(n)}(\omega_0)} \sim \frac{n}{2\pi^2} \quad \text{as } n \to \infty. \tag{62}$$

In summary, we have found three optimal threshold densities:

$$f^{(1)}(T) = Re^{-RT}, \tag{63}$$

$$f^{(2)}(T) = 2R2RTe^{-2RT}, \tag{64}$$

$$f^{(3)}(T) = 3R((3RT)^2/2)e^{-3RT}. \tag{65}$$

These are the only optimal solutions in the set $\{f^{(n)}\}$ and the departure from optimality gets progressively worse as $n \to \infty$. Undoubtedly, there are also many optimal solutions outside the set $\{f^{(n)}\}$.

The interesting point is that the three optimal solutions that we have found are as far as possible from the deterministic threshold density, which is obtained by letting $n \to \infty$. This qualitative result goes a long way towards explaining the stochastic character of the auditory code.

ACKNOWLEDGEMENTS: *The inner ear* In the sections on the fluid dynamics of the cochlea, I have taken the liberty of presenting my own work and that of my former student, Eli Isaacson. The reader who wants a less egocentric view of the field should consult the references.

Olof Widlund and Peter Lax have been particularly helpful to me in carrying out this work. The fluid dynamics of the inner ear is fun to talk

about, and I have also had helpful conversations with so many colleagues that it is difficult to remember them all. Here is a partial list. Alexandre Chorin, Ami Harten, Frank Hoppensteadt, Eugene Isaacson, Joe Keller, Michael Lacker, Cathleen Morawetz, John Neu, Stan Osher, Edward Peskin, Larry Sirovich, and Charles Steele.

Much of the computer programming connected with this project was done by Antoinette Wolfe. Computation was supported by the Department of Energy under Contract DE-AC02-76ER03077 at the Courant Mathematics and Computing Laboratory of New York University

The lecture on the stochastic auditory code relies heavily on Gestri's work. The beautiful fact that the expected value of the output is proportional to the expected value of the input for all threshold distributions is demonstrated in Gestri's paper Gestri also gives a verbal explanation of why stochastic coding may be preferable to deterministic coding in certain situations. The latter part of §7 is my attempt to formalize this idea.

References

1. J. B. Allen, *Two-dimensional cochlear fluid model: New results*, J. Acoust. Soc. Amer. **61** (1977), 110–119.

2. G. von Bekesy, *Experiments in hearing* (E. G. Weaver, trans.), McGraw-Hill, New York, 1960.

3. J. F. Brugge, D. J. Anderson, J. E. Hind and J. E. Rose, *Time structure of discharges in single auditory nerve fibers of the squirrel monkey in response to complex periodic sounds*, J. Neurophysiol. **32** (1969), 386–401.

4. J. D. Cole and R. S. Chadwick, *An approach to mechanics of the cochlea*, ZAMP **28** (1977), 785–804.

5. A. Dalcher, *Estimation in a stochastic model of neural activity*, Thesis, New York Univ., 1980.

6. G. Gestri, *Pulse frequency modulation in neural systems· A random model*, Biophysical J. **11** (1971), 98–109.

7 A. Inselberg and R. S. Chadwick, *Mathematical model of the cochlea*, SIAM J. Appl. Math. **30** (1976), 149–179.

8. Eli Isaacson, *A numerical method for a finite-depth, two-dimensional model of the inner ear*, Thesis, New York Univ., 1979.

9. N. Kiang, *Discharge patterns of single fibers in the cat's auditory nerve*, Research Monograph no. 35, M.I.T Press, Cambridge, Mass., 1965.

10. B. W Knight, *Dynamics of encoding in a population of neurons*, J. General Physiol. **59** (1972), 734–766.

11. _____, *The relationship between the firing rate of a single neuron and the level of activity in a population of neurons*, J. General Physiol. **59** (1972), 767–778.

12. _____, *Active response, tuning, and nonlinear tone mixture in the cochlea*, preprint, 1980.

13. M. B. Lesser and D. A. Berkley, *Fluid mechanics of the cochlea*. I, J. Fluid Mech. **51** (1972), 497–512.

14. C. C. Paige and M. A. Saunders, *Solutions of sparse indefinite systems of equations and least squares problems*, Report STAN-CS-73-399, Stanford Univ., 1973.

15. C. S. Peskin, *Partial differential equations in biology*, Courant Institute Lecture Notes, 1976, Chapter 5.

16. W M. Siebert, *Ranke revisited–a simple short-wave cochlear model*, J. Acoust. Soc. Amer. **56** (1974), 594–600.

17. C. R. Steele, *Behavior of the basilar membrane with pure tone excitation*, J. Acoust. Soc. Amer. **55** (1974), 148–162.

18. C. R. Steele and L. Taber, *Comparison of WKB and finite difference calculations for a two-dimensional cochlear model*, J. Acoust. Soc. Amer. **65** (1979), 1001–1006.

19. _____, *Comparison of WKB calculations and experimental results for three-dimensional cochlear models*, J. Acoust. Soc. Amer. **65** (1979), 1007–1018.